International Journal of Science and Engineering and Technology (IJSE) **Maiden Edition** www.federalpolyoko.edu.ng Volume 1; Issue 1; July 2025; Page No. 158-178.



### ENGINEERING A SMALL-SCALE NUT-CRACKING MACHINE: COMPUTATIONAL AND EXPERIMENTAL VALIDATION FOR RUBUS FRUTICOSUS PROCESSING

<sup>1</sup>Onu, John C., <sup>2</sup>Onyenanu, Ifeanyichukwu U. and <sup>3</sup>Anyene, Chinedu C. C. 1,3 Department of Agricultural Engineering, Federal Polytechnic, Oko, Anambra State, Nigeria <sup>2</sup> Department of Mechanical Engineering, Chukwuemeka Odumegwu Ojukwu University, Uli – Nigeria.

Corresponding Author: johnchibo@gmail.com

#### **Abstract**

Processing Rubus fruticosus nuts requires effective, environmentally friendly equipment to minimize mechanical damage and retain bioactive substances like anthocyanins and polyphenols. Advanced engineering solutions are required since traditional approaches frequently lead to inefficiency and nutrient loss. Through careful calculations for pulleys, shafts, and keys, this study sought to create a nut-cracking machine that was optimized for Rubus fruticosus nuts, with an emphasis on high cracking efficiency, little mechanical damage, and structural integrity. A mild steel frame of 600 mm by 400 mm by 500 mm, a "Type A" V-belt, and a 2 HP (1.492 kW) electric motor were all used in the design. Shaft diameter (70 mm), key length (100 mm), and pulley size (driver: 120 mm, driven: 240 mm) were all calculated. Frame integrity was evaluated using Autodesk Inventor 2023's Finite Element Analysis (FEA). Cutting, welding, and buying common parts like belts and bearings were all part of the fabrication process. The machine produced a torque of 12.344 N·m, a V-belt pitch length of 1201.42 mm, and a design horsepower of 1.939 kW. With a deflection of 2101.468 µm, the shaft withstands a maximum bending stress of 732.821 MPa and a shear stress of 36.061 MPa. A maximum frame displacement of 0.017 mm and a primary stress of 10.511 MPa were found using FEA, which is significantly less than the mild steel yield strength of 250 MPa. The strength of the key was ensured by its safety factor of 401.761. For processing Rubus fruticosus nuts on a small scale, the nut-cracking machine that was created is both efficient and structurally robust.

**Keyword**: Nut cracking machine, V-belt transmission, pulley design, shaft calculation, key specification.

#### Introduction

The design of Rubus fruticosus nut processing systems has attracted substantial attention in recent years due to the increased need for efficient, sustainable, and health-conscious food processing technology. Rubus fruticosus, generally known as blackberry, is a nutrient-dense fruit rich in bioactive substances such as polyphenols, flavonoids, and anthocyanins, which contribute to its antioxidant, antibacterial, and anti-inflammatory capabilities (Buczyński et al., 2024; Sik et al., 2024; Thanina et al., 2015). Recent advancements in food engineering and technology have focused on developing tools and procedures that can overcome the

disadvantages of traditional processing methods, such as nutrient loss, mechanical damage, and uneven heat distribution. For example, response surface methodology (RSM) has been used to optimize parameters like moisture content, weight, and speed in nut cracking processes, ensuring high cracking efficiency (up to 97.31%) and minimal mechanical damage (0.051). These health benefits have sparked interest in improving extraction and processing techniques to preserve these valuable compounds while increasing efficiency and yield (Thanina *et al.*, 2015; Wairegi, 2024). Similar to this, blackberry pomace has been improved for ultrasound-assisted extraction (UAE), which has produced excellent yields of anthocyanins (11.2 mg CGE/g) and total polyphenols (53.8 mg GAE/g) when 60% methanol, 20 minutes of extraction time, and 0.5% HCl acidification are used. 8. These developments demonstrate the trend toward precision engineering in food processing, where designs for frying chambers, stirrers, and heat exchangers are simulated and improved using computational tools such as computational fluid dynamics (CFD) and finite element analysis (FEA), guaranteeing consistent thermal distribution and structural integrity under operating loads (Dewir *et al.*, 2023; Thanina *et al.*, 2015).

The incorporation of automation and smart technology into *Rubus fruticose* nut processing has further changed the area. By simulating hand stirring motions, semi-automated devices using electric motors (such as the BS 63A 4 model, 0.12 kW, 1360 rpm) and gear-pulley systems have been developed to lower labour intensity while preserving product uniformity (Dursun et al., 2024; Thanina et al., 2015; Wairegi, 2024). In addition, the use of arbuscular mycorrhizal fungi (AMF) in cultivating Rubus fruticosus has shown promise in improving plant resilience and nutrient uptake during acclimatization, indirectly improving the quality of raw materials for processing (Dursun et al., 2024; Karp & Gasic, 2022). These advancements are complemented by the use of unconventional edible species and underutilized wild varieties, which offer untapped potential for diversifying product applications, such as functional muffins enriched with blackberry powder (10% incorporation rate) that boost antioxidant activity without compromising sensory acceptability (Buczyński et al., 2024; Sik et al., 2024). These systems frequently include LPG-powered burners for energy efficiency and aluminium alloy frying chambers (Al 5052) for optimal heat conductivity, achieving thermal efficiencies that reduce fuel consumption by up to 30% when compared to conventional methods, (Buczyński et al., 2024; Thanina et al., 2015).

In the processing of *Rubus fruticose* nuts, sustainability and scalability continue to be essential components of modern design paradigms. Through the use of water-efficient extraction methods, waste valorisation (such as pomace microcapsules for dairy products), and renewable energy integration, life cycle evaluations (LCA) of these systems have a strong emphasis on lowering carbon footprints (Buczyński *et al.*, 2024; Meng *et al.*, 2022; Sik *et al.*, 2024). Fermented blackberry juices made with Limosilactobacillus fermentum FUA033, for instance, have been shown to decrease post-harvest deterioration and increase the bioavailability of urolithin A, a metabolite having anti-aging qualities (Buczyński *et al.*, 2024; Wairegi, 2024). Invasive Rubus species have also been mapped thanks in large part to community-driven initiatives and citizen science projects, which have informed ecological management plans that strike a compromise between biodiversity protection and agricultural productivity (Dinu, 2020; Tu, 2024). In order to satisfy nutritional, economic, and environmental goals, the design of *Rubus fruticose* nut processing systems must continue to advance as the demand for functional foods rises globally. This evolution must make use of multidisciplinary research in genomics, metabolomics, and AI-

driven automation. In order to provide fair access to the advantages of technology, future initiatives include CRISPR-based cultivar improvement, blockchain-enabled supply chain transparency, and decentralized micro-processing units designed for small-scale farmers (Bhatt et al., 2023; Buczyński et al., 2024; Meng et al., 2022). This all-encompassing strategy highlights how engineered solutions may fully exploit the benefits of Rubus fruticosus nuts for sustainability, industry, and health.

In conclusion, food science, engineering, and sustainability are dynamically intersected in the design of Rubus fruticosus nut processing systems. Significant advancements have been made recently in the optimization of mechanical, thermal, and biochemical processes to increase productivity, protect bioactive substances, and lessen environmental effect. These developments, which range from RSM-optimized cracking machines to AMF-enhanced cropping and UAEbased extractions, are part of a larger movement in food technology toward sustainability and accuracy. In addition to tackling global issues in nutrition security and ecological preservation, the combination of smart technologies, renewable energy, and community participation guarantees that these developments are inclusive and scalable. To fully use Rubus fruticose nuts and open the door to more sustainable and healthful food systems, interdisciplinary cooperation will be crucial as the subject develops.

#### 2. **Literature Review**

Although the research on Rubus fruticose and related species shows creative ways to use natural qualities for technological and biological breakthroughs, it also highlights a conflict between methodological constraints and real-world applications. In order to overcome the difficulty of delicate maturity cues in Rubus fruticosus, Olisah et al. (2024) offer a multi-input CNN ensemble classifier for identifying blackberry ripeness using hyperspectral imaging. This classifier achieves 90.2% accuracy in the field and 95.1% accuracy in controlled conditions. However, scalability over a range of farm circumstances may be limited by the model's dependence on certain Vis-NIR wavelengths (700 nm, 770 nm). Monteiro et al. (2021, 2023), on the other hand, concentrate on biomimetic PCL membrane imitating. Although the leaf topography of Rubus fruticose shows improved osteogenic differentiation of rBMSCs for bone regeneration, their method is not validated in vivo and has difficulties scaling complicated natural topographies for clinical usage. The study's specificity to a single plant limits its generalizability in comparison to Yan et al. (2021) ball mill-assisted extraction method for Rubi Fructus phenolics, which achieves high recovery rates (98.7–102%) but is limited by the complexity and expense of HPLC analysis. Ganachari et al. (2024) offer detailed engineering considerations for Asparagus racemosus processing machinery, providing precise physical and textural data to optimize design. Although each research pushes the envelope in its field, context-specific limitations and insufficient validation limit their practical significance, highlighting the need for more reliable, scalable solutions.

#### 3. Materials and methods

#### **Description of the machine**

In small to medium-sized agricultural settings, the nut-cracking machine is a reliable, mechanically effective equipment made for high-performance processing of several nut varieties, including peanuts, walnuts, and almonds. With a mild steel frame which is 600 mm (L) x 400 mm (W) x 500 mm (H), supporting a hardened steel crushing drum consisting of a rotor and stator and powered by a 2 HP (1.492 kw) single-phase electric motor, the nut-cracking machine is a sturdy little device made for effective nut processing. A "Type A" V-belt and cast-iron pulley system conveys power, reducing the speed from 1500 rpm to 750 rpm. A stainless-steel collector collects broken nuts, and stainless-steel hinges and a mild steel top that has been welded together provide secure access and trash control. A 70 mm stainless steel shaft is supported by two pillow block bearings and fastened with structural steel keys to guarantee smooth operation. The components of the machine are outlined in Table 1.

TD 11	1		C .1	nut-cracking	1 .
Lable	١.	Components	COTTHE	nut_cracking	machine
1 autc	1.	Component	ou unc	mut-cracking	macmin

S/N	Components	Quantity	Material
1	Frame	1	Mild Steel
2	Hinge	2	Stainless Steel
3	belt	1	Rubber (V-belt Type A)
4	Bolt	14	High-Strength Steel
5	Nut	14	High-Strength Steel
6	Pillow block bearing	2	Cast Iron
7	Pulley	2	Cast Iron
8	Welded cover	1	Mild Steel
9	Electric motor	1	Standard Motor Assembly
10	collector	1	Stainless Steel
11	key	2	Structural Steel
_12	Crushing drum (rotator and stator)	1	Hardened Steel

### 3.2 Working principle

The electric motor's rotational energy is transformed into mechanical force by the nut-cracking machine to crack nuts. For maximum torque, the motor reduces speed to 750 rpm by driving a cast iron driver pulley that is coupled to a bigger driven pulley by a "Type A" V-belt. The hardened steel rotor inside the crushing drum is rotated by this driven pulley, which is keyed to a stainless-steel shaft. The revolving rotor and stationary stator use compressive and shear forces to fracture the shells after nuts are fed into the drum through a hole in the welded cover.

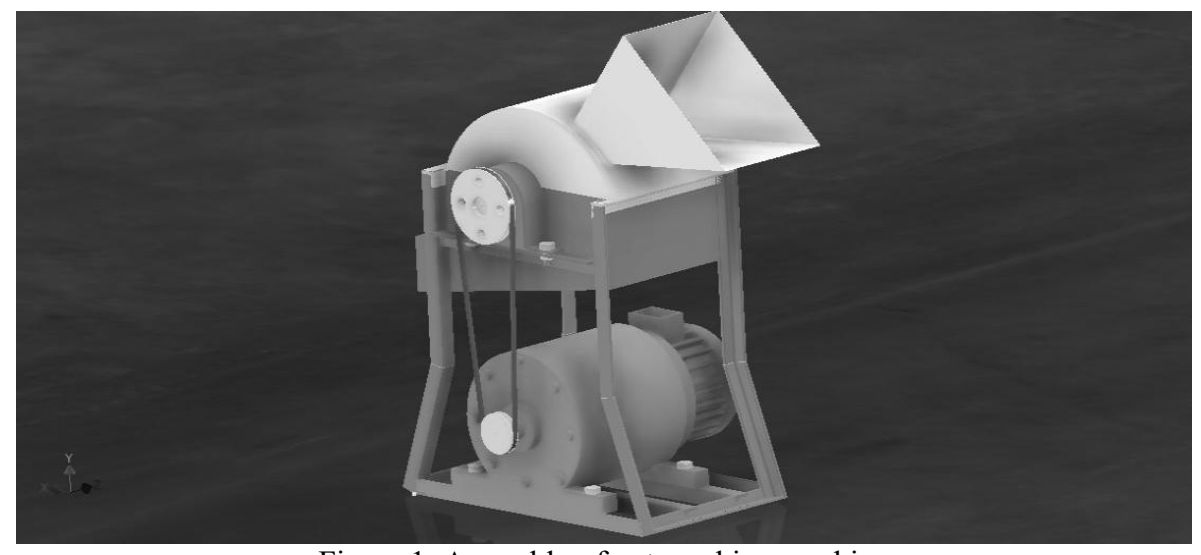


Figure 1: Assembly of nut cracking machine

### 3.3 Design approach

Establishing machine requirements, including performance objectives and limitations, is the first step in the design process. Durability is therefore guaranteed by material selection (stainless steel for the shaft). After designing the essential parts (pulleys, shaft, and drum), calculations are made (torque, stress). Before prototyping, safety and efficiency are confirmed by analysis (FEA, kinematics) and CAD drawings that represent the assembly, which is summarised in Figure 2.

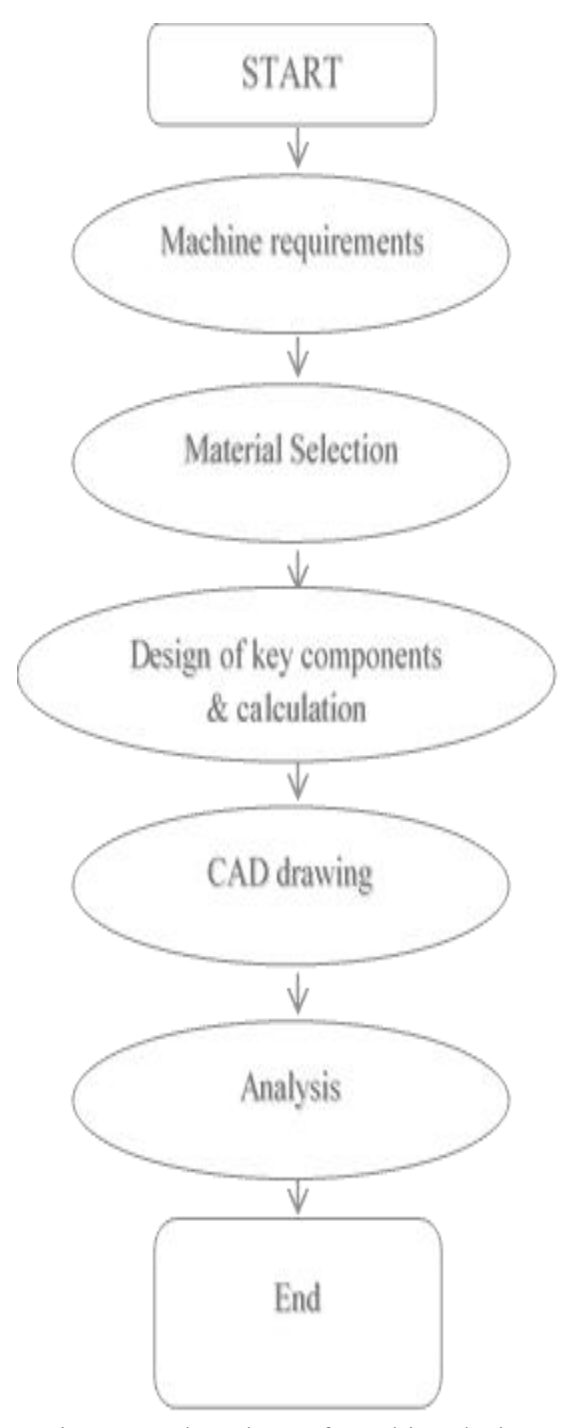


Figure 2: Flowchart of machine design

### 3.4 Design consideration

Safety, simplicity of installation, corrosion resistance, and material strength are important factors. The shaft diameter was determined to support combined bending and torsional stresses, and the V-belt was chosen for effective power transmission (Onyenanu et al., 2023). engineering procedures and rules were followed throughout the design.

3.5 Description of parts							
Part Name	Description	<b>Technical Details</b>	Figure				
Collector	Collects broken nuts and shell pieces; ensures sanitary processing.	- Material: AISI 304 stainless steel - Dimensions: 300 mm (L) × 200 mm (W) × 150 mm (H) - Capacity: 5 L - Weight: 2 kg - Attachment: Bolted/slide-in.	Figure 3:				
Welded Cover	Encloses the crushing drum; protects operators from debris.	- Material: ASTM A36 mild steel - Dimensions: 400 mm (L) × 300 mm (W) × 200 mm (H) - Yield strength: 250 MPa - Weight: 5 kg - Attachment: Hinged latch.	Figure 4:				
Crushing Drum	Breaks nuts via rotor-stator assembly; hardened for wear resistance.	- Material: AISI 4140 hardened steel - Rotor diameter: 200 mm - Stator dimensions: 250 mm (L) × 200 mm (W) - Hardness: 50–55 HRC - Weight: 10 kg.	Figure 5:				
Electric Motor	Powers the drum via pulley system (2 HP induction motor).	- Type: Single/three-phase induction - Power: 1.492 kW (2 HP) - Speed: 1500 RPM - Voltage: 220–240 V - Mounting: M10 bolts.	Figure 6:				

Engineering A Small-Scale Nut-Cracking Machine: Computational and Experimental Validation for *Rubus Fruticosus*Processing

Part Name	Description	<b>Technical Details</b>	Figure
Belt	Transfers power from motor to drum (V-belt).	- Type: A60 V-belt (ANSI/RMA IP-20) - Length: 1557.02 mm - Width: 12.7 mm - Max speed: 30.48 m/s - Power rating: 2.856 kW.	Figure 7:
Frame	Structural base; supports all components (I. U. Onyenanu & Erhimona, 2023).	- Material: ASTM A36 mild steel - Dimensions: 600 mm (L) × 400 mm (W) × 500 mm (H) - Yield strength: 250 MPa - Weight: 20 kg.	Figure 8:
Pillow Block Bearing	Supports shaft rotation; reduces friction (Okpala et al., 2025).	cast iron (housing)	Section A-A SCALE .6: 1
Pulley Wheels	Transmits motion via V-belt; includes driver and driven pulleys (Ukwu et al., 2024).	- Belt type: V-belt (40° wedge angle) - Classifications: Type A–E - Included angle: 30°–40° (standard).	Figure 10:

### 3.6 Design calculation for the pulley wheels

A pulley is a vital part used in most belt transmission engines. It is a collection of one or more wheels tensioned with belts or ropes, which are used to overcome considerable weights and loads. In practice, there are different classifications of pulleys, ranging from their types to and diameter sections. The type of belt used for this design is the V-belt. According to (Long *et al.*, 2020)The V-belts are usually made of fabric or rubber, with an included angle of 30<sup>0</sup> and 40<sup>0</sup>. There are five types of V-belts, which are Type A, Type B, Type C, Type D, and Type E.

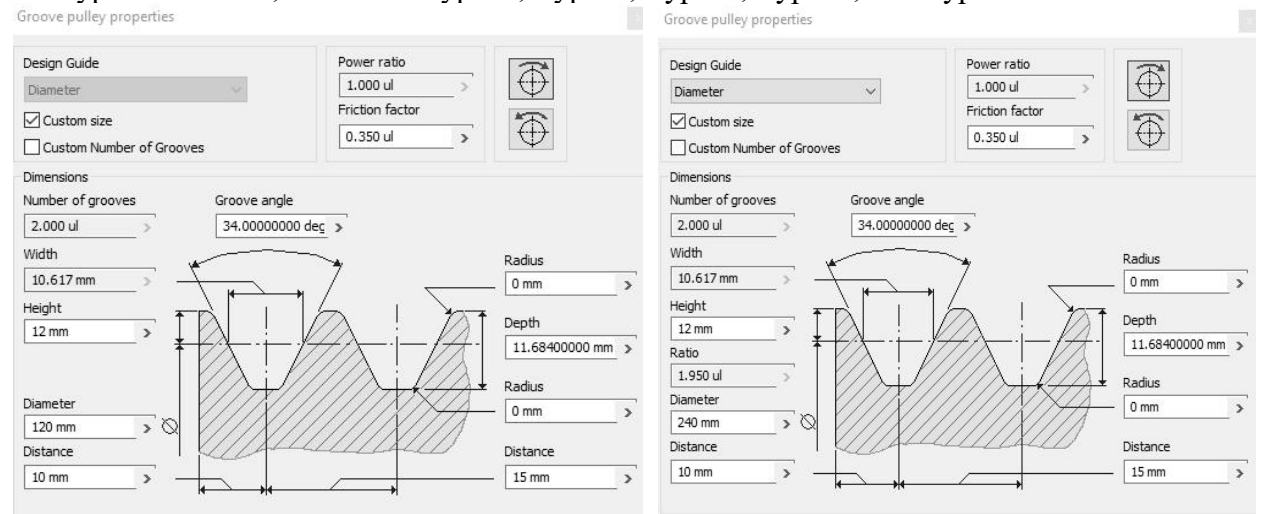


Figure 11: Cross-section of the V-grooved [A] driver and [B] driven pulley

• To derive the nature, strength, and type of belt used for the design processes, the design Horsepower and speed of the driver motor are taken into consideration. Mathematically, the Horsepower (Hp) is calculated as:

Design Hp 
$$\times$$
 K<sub>S</sub>

Where, Input Hp = Motor horsepower (2 Hp)

K<sub>S</sub> = Service Factor (1.3)

Then,

Design Hp = 
$$2 \times 1.3 = 2.6$$
 Hp

Therefore, the belt used for the design is a Type A belt, with 2 grooves

• Then the relative speeds of the driving motor and the driven pulley are then calculated. Mathematically, the Speed ratio is expressed as:

Speed ratio = 
$$\frac{\text{Driving speed}}{\text{Driven speed}}$$
 2.  
 $\frac{1500}{750} = 2/1 = 2:1$ 

• Let the diameter of the driving pulley wheel be 120 mm according to the Indian Standards, as cited by (Long *et al.*, 2020). Then the diameter of the driven pulley can be calculated as:

$$\frac{D}{d} = \frac{n}{N}$$

Where, D = diameter of the driven pulley

d = diameter of the driving pulley

n =speed of the driving pulley

N =speed of the driven pulley

$$\frac{D}{120} = \frac{1500}{750} = 240 \text{ mm}$$

Therefore the diameter of the driven pulley is 240 mm

• The centre distance between the two pulleys be 350 mm. The nominal pitch length of the belt can be gotten mathematically using the equation;

$$L = 2c + \frac{\pi}{2}(D+d) + \frac{(D-d)^2}{4c}$$
 4.

Where, L = nominal pitch length of belt

c = centre distance between the two pulleys

D = diameter of the driven pulley

d = diameter of the driving pulley

Then, L = 
$$2 \times 350 + \frac{\pi}{2}(240 + 120) + \frac{(240 - 120)^2}{4 \times 350}$$
  
L =  $700 + 565.4867 + 10.2857$   
L =  $1275.7724$  mm

The overall standard length of "Type A" belt selected for the design is 1201.420 mm (available standard belt length).

• To obtain the actual centre distance between the two pulleys. Taking the assumed centre distance to be 350 mm. The mathematical relationship used is:

$$c = A + \sqrt{A^2 - B}$$
 5. Also, 
$$A = \frac{L}{4} - \pi \frac{(D+d)}{8} = \frac{1275.7724}{4} - \pi \frac{(240+120)}{8} = 177.5714 \text{ mm}$$
 
$$B = \frac{(D-d)^2}{8} = \frac{(240-120)^2}{8} = 1800 \text{ mm}$$
 
$$c = 177.5714 + \sqrt{(177.5714)^2 - 1800} = 349.99 \text{ mm}$$

Table 2 presents the technical specification of the pulley wheels.

Table 2: The technical specification of the pulley wheels

Item	Abbreviation/Symbol	Specification
Display name		V-Belt ANSI/RMA IP-20
Size		A60
Number of belts	Z	2.000 ul
Wedge angle	α	40.00 deg
Width	Ъ	12.700 mm
Height	h	7.938 mm
Datum width	$b_{\mathrm{w}}$	10.617 mm
Datum length	$L_{d}$	1557.020 mm
External length	$L_{e}$	1573.873 mm
Internal length	$L_{i}$	1524.000 mm
Length correction factor	$c_3$	0.970 ul
External line offset	$\mathrm{H}_{\mathrm{w}}$	2.682 mm
Pitch line offset	a	3.175 mm
Minimum pulley datum diameter	$\mathrm{D}_{\mathrm{wmin}}$	76.200 mm
Maximum flex frequency	$ m f_{max}$	60.000 Hz
Maximum belt speed	V <sub>max</sub>	30.480 mps
Specific mass	m	0.104  kg/m
Base power rating	$P_{ m RB}$	2.856

Table 3 presents the calculated strength check of the grooved pulley wheels

Table 3: Calculated strength of the grooved pulley

Parameter	Abbreviation/Symbol	Specification
Power	P	1.939 kW
Torque	T	12.344 N m
Speed	n	1500.000 rpm
Efficiency torque factor	$\eta_t$	0.980 ul
Efficiency	η	0.975 ul
Belt slip	S	0.006 ul
Arc of contact correction factor	$\mathbf{c}_1$	0.967 ul
Service factor	$\mathbf{c}_2$	1.300 ul
Resultant service factor	$c_{PR}$	2.693 ul
Length correction factor	<b>c</b> <sub>3</sub>	0.970 ul
Number of belts correction factor	<b>C</b> 4	0.975 ul
Number of pulleys correction factor	c <sub>5</sub>	1.000 ul
Modify friction with speed factor	$ m f_{mod}$	0.012  s/m
Tension factor	$\mathbf{k}_1$	1.500 ul
Belt Speed	V	9.924 mps
Belt flex frequency	$\mathrm{f_{b}}$	12.747 Hz
Number of belts required	Zer	0.966 ul
Effective pull	$F_p$	195.395 N
Centrifugal force	$\overline{F_c}$	20.517 N
Belt installation tension	$F_t$	116.393 N
Maximum tension in belt span	$F_{tmax}$	165.242 N

### 3.7 **Design calculation for the shaft**

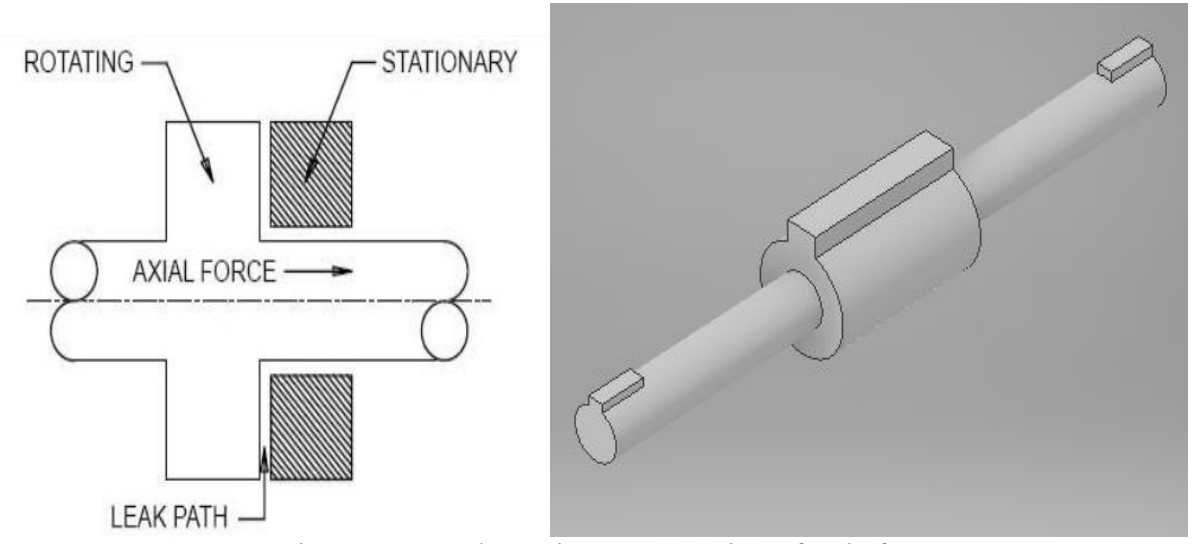


Figure 12: A schematic representation of a shaft

A shaft is a structural member that help in transmitting power from a section of a machine to another. A shaft usually experiences a rotary motion during operation. When a shaft is subjected to both bending and twisting moments, then the moment experienced in the shaft can be explained by;

$$T_e = \sqrt{(K_m \times M)^2 + (K_t \times T)^2} = \frac{\pi}{16} \times \tau(d)^3$$
 6.

$$_{\text{and}} T = \frac{P \times 60}{2\pi \times N}$$
 7.

Where,  $T_e$  = Equivalent twisting moment

T = Torque transmitted by the shaft

M = Bending moment of the shaft

P = Power to be transmitted by the shaft (1938.82 W)

N =Speed of the shaft (750 rpm)

 $K_m$  = Combined shock and fatigue for bending (i.e. 2)

 $K_t$  = Combined shock and fatigue for torsion (i.e. 2)

d = Diameter of the shaft

 $\tau$  = Allowable shear stress of 42 MPa; then the Torque to be transmitted by the shaft can be computed:

The shaft in this design is acted upon by a load which is uniformly distributed along its axis of 251.5 mm (taking reference from the middle or centre point). Therefore, the Maximum bending moment (M) of shaft with total length of 428 mm can be resolved considering the uniform load.

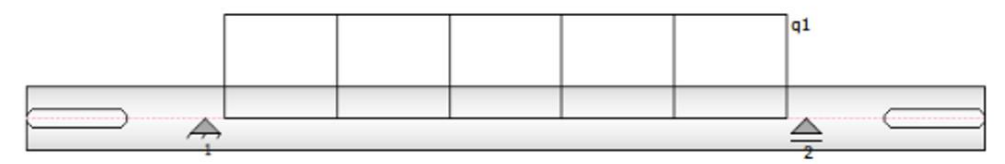


Figure 13: 2D Sketch of continuous load and relative force acting on the shaft

Let  $R_v$  and  $R_x$  be reactions at position y and x respectively.

Let a continous Load of  $176.58 \frac{N}{mm}$  act at the center of the beam with length of 251.5 mm Where all upward forces equal downward forces, then;

$$R_v + R_x = 44409.87N$$

Let; 
$$\mathcal{E}_{Rx} = 0$$

$$R_y \times 268 = 44409.87 \times 134$$

$$R_y = \frac{5950922.58}{268}$$

$$R_v = 22.204 \text{ KN}$$

$$R_x = 44409.87 - R_y$$

$$R_x = 44409.87 - 22204.935$$

$$R_x = 22.204KN$$

Table 4 presents the technical specification of the shaft

Table 4: Technical specification of the shaft

Item	Specification
Diameter	70 mm
Material	Stainless Steel
Modulus of Elasticity	190000 MPa
Shear Displacement Ratio	1.188 ul
Number of Divisions	1000 ul
Mode of reduced stress	НМН
Modulus of Rigidity	73000 MPa
Specific material density	8030 kg/m3
Keyway Length	45 mm
Width of the key	8 mm

Table presents the reaction loads at each index locations

Table 5: The reaction loads at each index locations

Index	Location	Continuous Load De					Deflection			
		Y	X	Size	Direction	Length	Y	X	Size	Direction
q1	88.25 mm	9	176.580	176.580	90.000	251.500	33 <b>7</b> 5	2.5	207.157	269.99°
->:=:			N/mm	N/mm		mm	0.028	207.157	μm	
							μm	μm		7610000000
	339.75 mm						33 <del>4</del> 3	<u> </u>	207.408	269.99°
							0.028	207.408	μm	
							μm	μm	201-010	

Table 6 presents the resolved results for the shaft

Table 6: Resolved Results for the Shaft

Parameters	Unit	Specification
Length	L	428.000 mm
Mass	Mass	2.116 kg
Maximal Bending Stress	$\sigma_{\mathrm{B}}$	732.821 MPa
Maximal Shear Stress	$ au_{\mathrm{S}}$	36.061 MPa
Maximal Torsional Stress	τ	0.000 MPa
Maximal Tension Stress	$\sigma_{T}$	0.000 MPa
Maximal Reduced Stress	$\sigma_{red}$	732.821 MPa
Maximal Deflection	$f_{\text{max}}$	2101.468 microm
Angle of Twist	φ	0.0 eg

Below are the diagrammatic representations of the reactions experienced in the shaft.

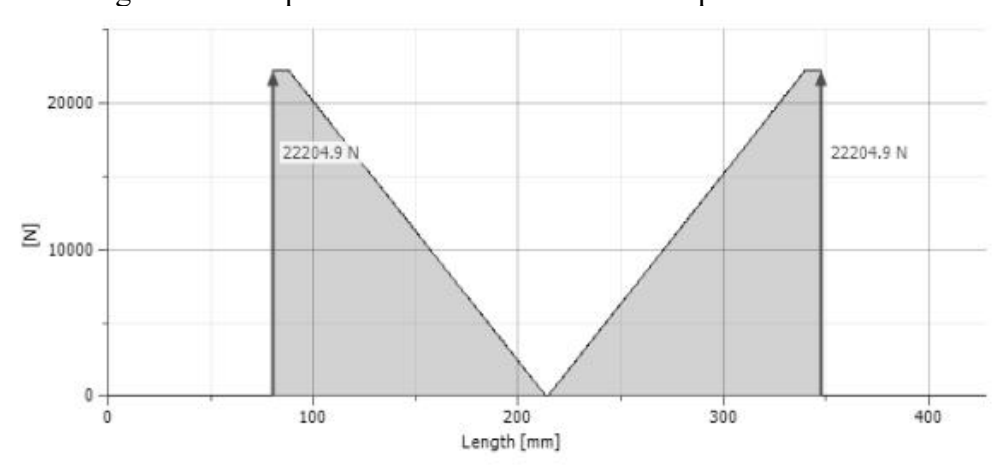


Figure 14: The shear force diagram

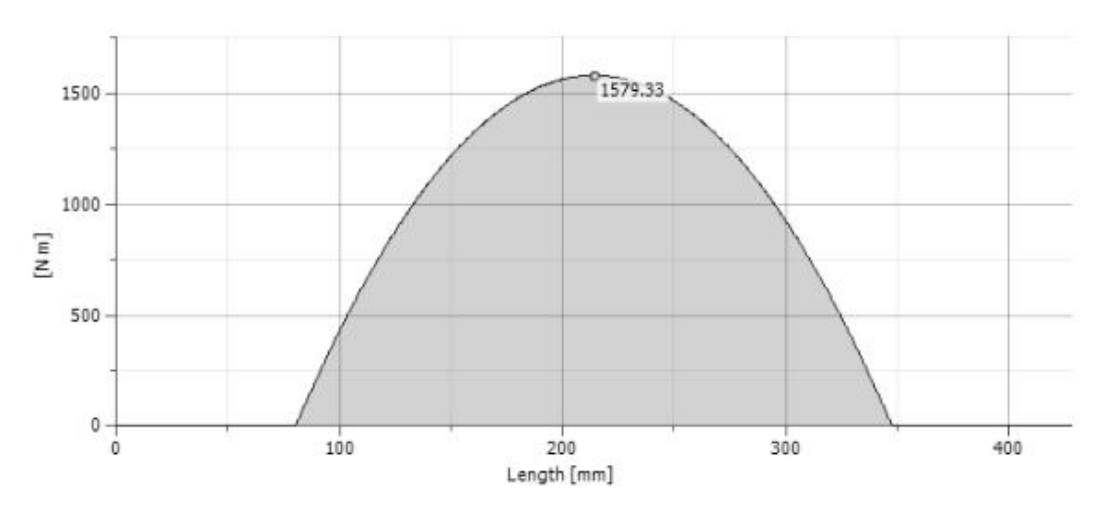


Figure 15: The bending moment diagram

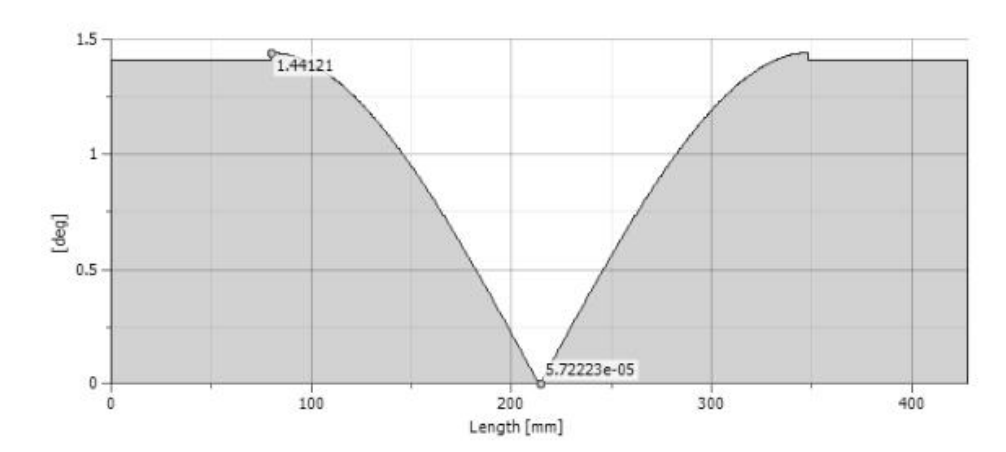


Figure 16: The deflection angle diagram

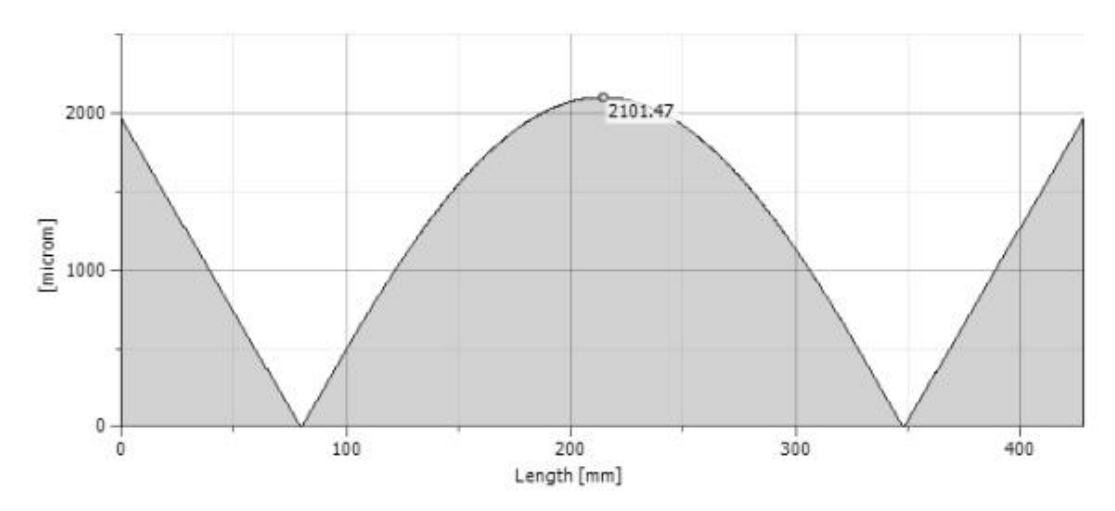


Figure 17: the deflection diagram

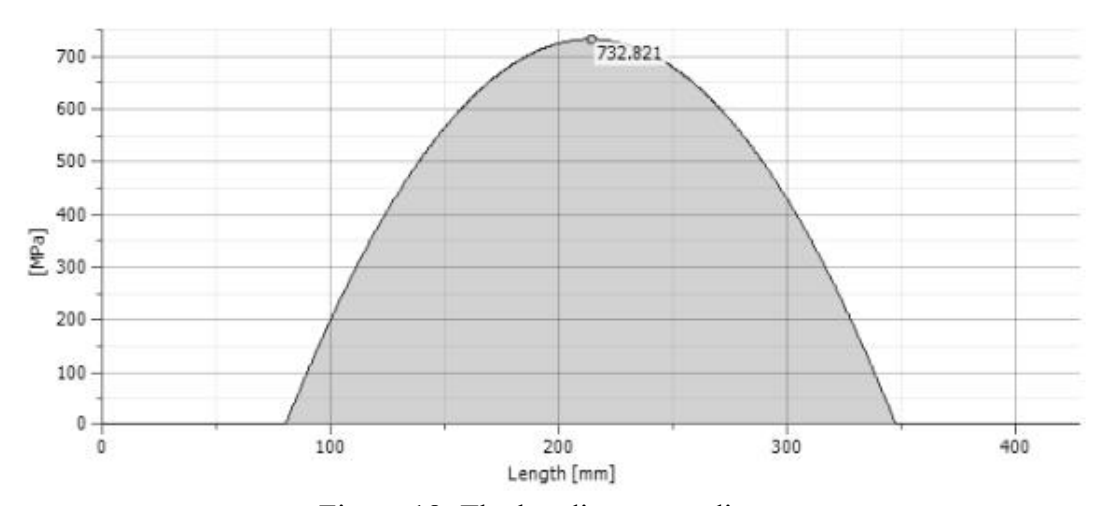


Figure 18: The bending stress diagram

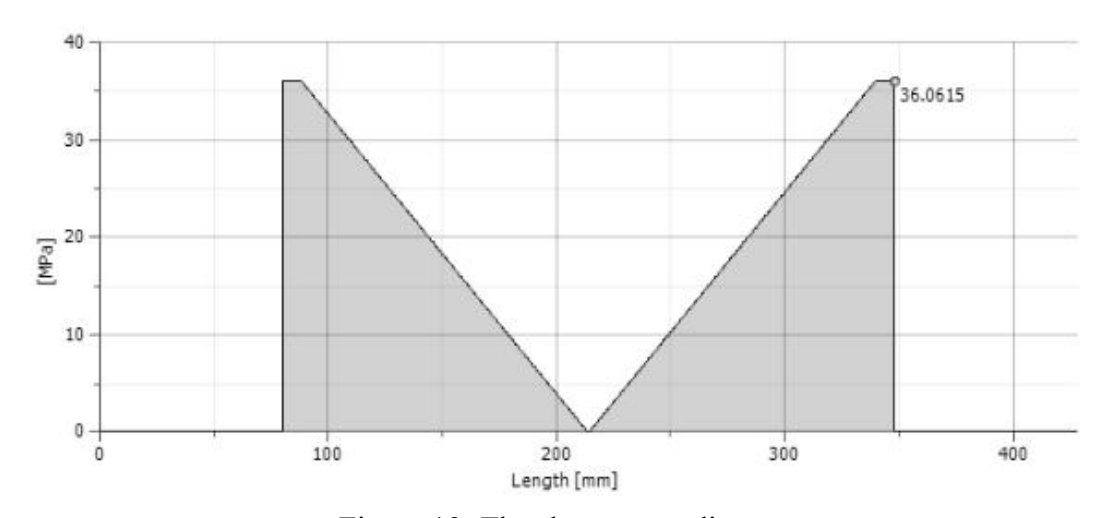


Figure 19: The shear stress diagram

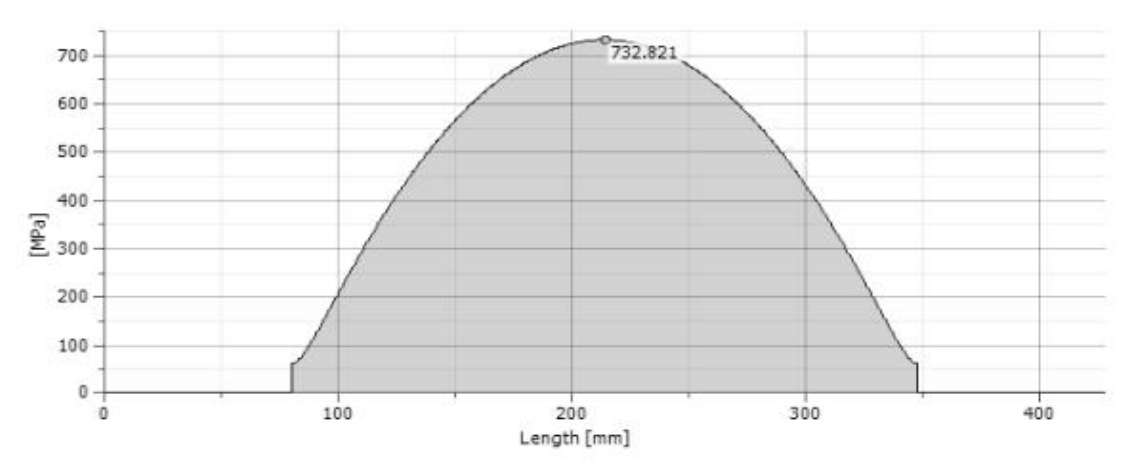


Figure 20: The reduced stress

### 3.8 Design calculations for the length of the sunk key

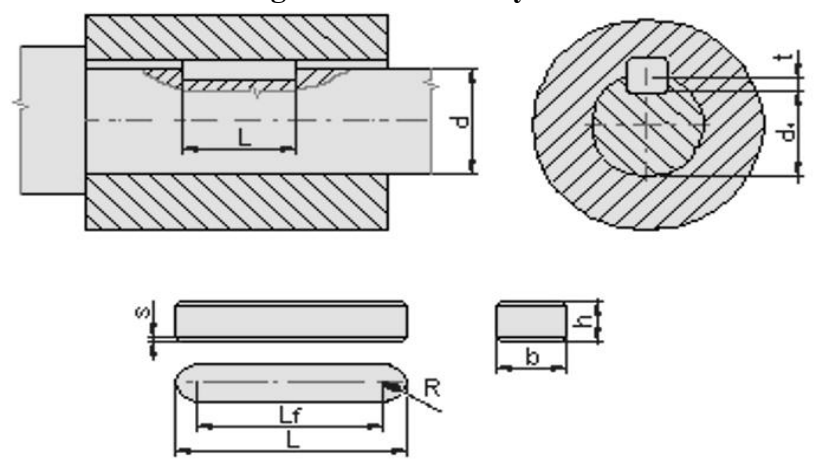


Figure 21: Schematic representation of rectangular sunk key

Maintaining the standard dimensions of a rectangular sunk key for a shaft, we can assume that the width the key keeping relationships with the dimensions of the shaft be 14 mm. Then, the length of the key taken to be same as the length of the hub. Mathematically, the length of the sunk key is taken as;

 $L = 1.5 \times d$ 

 $L = 1.5 \times 70 = 105 \text{ mm}$ 

According to the Standard Units and Availability criteria assume  $L=100\ mm$ 

Where, L = Length of the key

d = Diameter of the shaft (70 mm)

Table 7 presents the technical specification of the key

Table 7: The technical specification of the key

Item	Unit	Specification
Material		Structural steel
Allowable Pressure	P	246.00 MPa
Key Width	b	20.000 mm
Key Height	h	8.000 mm
Key Length	1	100.000 mm
Functional Length	$1_{\mathrm{f}}$	80.000 mm
Key Chamfer	S	0.400 mm
Key Radius	R	0.160 mm
Minimum Functional Key Length	$\mathcal{L}_{min}$	0.199 mm
Minimum Shaft Diameter	$d_{\min}$	4.504 mm
Calculated Pressure for Key	$P_c$	0.612 MPa
Safety of Key	S	401.761 ul
Calculated Pressure for the Shaft	$P_c$	0.612 MPa
Safety of Shaft	S	401.761 ul
Calculation Pressure of the Hub	$P_{c}$	0.612 MPa
Safety of the Hub	S	401.761 ul

### 3.9 Fabrication process

To ensure accuracy, robustness, and worth, the nut-cracking machine's components are produced and assembled through a sequence of manufacturing stages (Onyenanu & Erhimona, 2023). The fabrication process for each component is shown in the table below, along with the particular fabrication process and equipment.

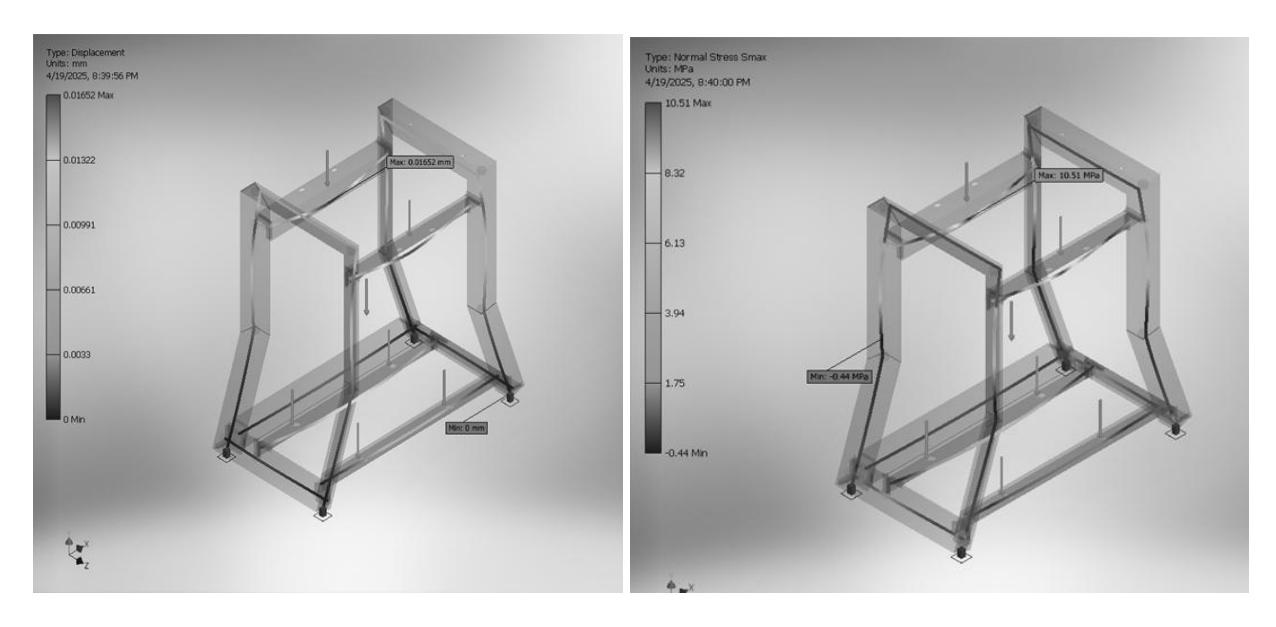
Table 8: fabrication process for each component listed

S/N	Component	Material	Fabrication Process	Tools/Equipment
1	Frame	Mild Steel	Cutting, welding, drilling, and painting.	Angle grinder, welding machine, drill press, paint sprayer.
2	Hinge	Stainless Steel	Cutting, bending, drilling, and polishing.	Metal shear, press brake, drill press, polishing wheel
3	Belt	Rubber (Type A V-belt)	Purchased	-
4	Bolt	High-Strength Steel	Purchased	-
5	Nut	High-Strength Steel	Purchased	-
6	Pillow Block Bearing	Cast Iron (housing), Steel (bearing)	Purchased	-
7	Pulley	Cast Iron	Purchased	-
8	Welded Cover	Mild Steel	Cutting, bending, welding, drilling and painting.	Metal shear, press brake, welding machine, drill press, paint sprayer
9	Electric Motor	Standard Motor Assembly	Purchased	-
10	Collector	Stainless Steel	Cutting, bending, welding, polishing, and drilling.	Metal shear, press brake, welding machine, polishing wheel, drill press
11	Key	Structural Steel	Cutting, milling, chamfering, and heat-treating.	Band saw, milling machine, chamfer tool, heat treatment furnace
12	Crushing Drum	Hardened Steel	Forging, turning, hardening and grinding.	Forging press, CNC lathe, heat treatment furnace, grinding machine

### 4.0 Result and analysis

The structural integrity of the nut-cracking machine's frame was evaluated using Finite Element Analysis (FEA) in Autodesk Inventor 2023, with results summarized in a static analysis table. The analysis revealed a maximum displacement of 0.017 mm and a minimum of 0.000 mm, indicating minimal deformation under operational loads. Forces acting on the frame ranged from

-155.987 N to 171.844 N (Fx), -155.945 N to 179.523 N (Fy), and -42.185 N to 250.289 N (Fz). Moments varied significantly, with Mx ranging from -21406.148 N mm to 10443.509 N mm, My from -10287.568 N mm to 21553.881 N mm, and Mz from -73.553 N mm to 74.758 N mm. Normal stresses included a maximum principal stress (Smax) of 10.511 MPa and a minimum (Smin) of -5.816 MPa, with axial stress (Saxial) between -0.789 MPa and 0.133 MPa. Shear stresses (Tx, Ty) ranged from -1.573 MPa to 1.367 MPa, and torsional stresses (T) varied from -0.332 MPa to 0.327 MPa. These results, visualized in Figure 22a, Figure 22b and Figure 23 confirm the frame's robustness, with stresses well below the yield strength of mild steel (250 MPa), ensuring reliable and safe operation for small-scale nut processing.



(a) Figure 22: Frame analysis result: (a) Displacement (b) Normal stress

(b)

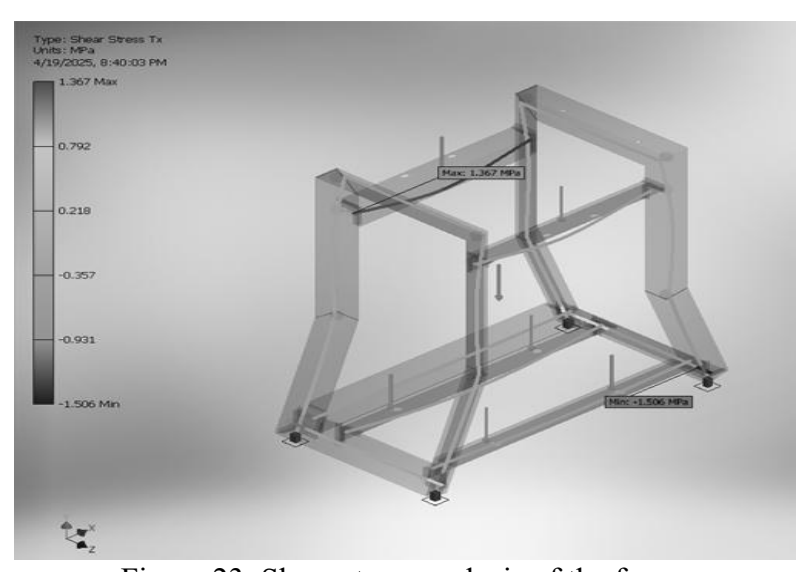


Figure 23: Shear stress analysis of the frame

Table 9: Static Result Summary in Autodesk Inventor 2023

Name	•	Minimum	Maximum
Displacement		0.000 mm	0.017 mm
Forces	Fx	-155.987 N	171.844 N
	Fy	-155.945 N	179.523 N
	Fz	-42.185 N	250.289 N
Moments	Mx	-21406.148 N mm	10443.509 N mm
	My	-10287.568 N mm	21553.881 N mm
	Mz	-73.553 N mm	74.758 N mm
Normal Stresses	Smax	-0.444 MPa	10.511 MPa
	Smin	-5.816 MPa	-0.069 MPa
	Smax(Mx)	0.000 MPa	10.393 MPa
	Smin(Mx)	-5.070 MPa	-0.000 MPa
	Smax(My)	0.000 MPa	10.464 MPa
	Smin(My)	-4.995 MPa	-0.000 MPa
	Saxial	-0.789 MPa	0.133 MPa
Shear Stresses	Tx	-1.506 MPa	1.367 MPa
	Ty	-1.573 MPa	1.366 MPa
Torsional Stresses	T	-0.332 MPa	0.327 MPa

#### 5.0 Conclusion

Key outcomes include a 2 HP (1.492 kW) single-phase electric motor running at 1500 rpm and reducing it to 750 rpm using a "Type A" V-belt with a nominal pitch length of 1201.42 mm, resulting in a design horsepower of 1.939 kW. Supported by a centrifugal force of 20.517 N and a belt tension of 165.242 N, the pulley system, which had a driven pulley diameter of 240 mm and a driver pulley diameter of 120 mm, transmitted a torque of 12.344 N·m. When exposed to a maximum bending moment of 251.5 mm, the 70 mm stainless steel shaft showed a maximum bending stress of 732.821 MPa, a shear stress of 36.061 MPa, and a deflection of 2101.468 µm. All of these values were within acceptable bounds for the material's permissible shear stress of With a length of 100 mm and a width of 20 mm, the rectangular buried key 42 MPa. demonstrated its dependability under operating loads by achieving a safety factor of 401.761. Key outcomes include a 2 HP (1.492 kW) single-phase electric motor running at 1500 rpm and reducing it to 750 rpm using a Type A V-belt with a nominal pitch length of 1201.42 mm, resulting in a design horsepower of 1.939 kW. Supported by a centrifugal force of 20.517 N and a belt tension of 165.242 N, the pulley system, which had a driven pulley diameter of 240 mm and a driver pulley diameter of 120 mm, transmitted a torque of 12.344 N·m.

#### 6.0 **Recommendation**

Future enhancement suggestions include using Internet of a Things-based sensors to track performance indicators in real time, such mechanical damage and cracking efficiency, in order to maximize operations. The machine's lifespan might be increased by investigating cutting-edge corrosion-resistant coatings for the mild steel parts, especially in humid agricultural settings. Furthermore, adding variable speed controls to the motor could improve flexibility by enabling adaptation to various nut types. Field testing is necessary to validate the machine's performance in real-world scenarios and make sure it achieves the desired mechanical damage of 0.051 and cracking efficiency of up to 97.31%, as stated in previous research. These improvements would

increase the machine's scalability for wider agricultural uses and bring it into line with environmental aims.

#### Reference

- Bhatt, S. C., Naik, B., Kumar, V., Gupta, A. K., Kumar, S., Preet, M. S., Sharma, N., & Rustagi, S. (2023). Untapped potential of non-conventional rubus species: Bioactivity, nutrition, and livelihood opportunities. *Plant Methods*, *19*(1), 114. https://doi.org/10.1186/s13007-023-01094-y
- Buczyński, K., Kapłan, M., & Jarosz, Z. (2024). Review of the Report on the Nutritional and Health-Promoting Values of Species of the Rubus L. Genus. *Agriculture*, *14*(8), Article 8. https://doi.org/10.3390/agriculture14081324
- Dewir, Y. H., Al-Qarawi, A. A., Alshahrani, T., Bansal, Y., Mujib, A., Murthy, H. N., Alebidi, A. I., Almutairi, K. F., & Al-Saif, A. M. (2023). *Influence of Arbuscular Mycorrhizal Fungi on the Growth and Development of Micropropagated Rubus fruticosus 'P45' Plants during Acclimatization*. https://doi.org/10.21273/HORTSCI17211-23
- Dinu, G. (2020). Preliminary research on the proximate composition of blackberry fruits (Rubus fructicosus).

  https://www.academia.edu/70902507/Preliminary\_research\_on\_the\_proximate\_compositi on of blackberry fruits Rubus fructicosus
- Dursun, S. K., Taşova, M., Dinçer, E., & İşbilir, M. E. (2024). Assessment of carrier agents in terms of physicochemical, energy analyses and bioactive constituents of blackberry (*Rubus fruticosus* L.) powder processed by convective and hybrid drying methods. *Heat and Mass Transfer*, 60(10), 1699–1712. https://doi.org/10.1007/s00231-024-03516-6
- Ganachari, A., R., Mathad, P. F., Nidoni, U., Shirwal, S., & Reddy, M. (2024). Engineering considerations for designing processing machinery for *Asparagus racemosus* roots. *Current Science*, 127(8), 957. https://doi.org/10.18520/cs/v127/i8/957-962
- Karp, D., & Gasic, K. (2022). Register of new fruit and nut cultivars list 51. *HortScience*, 57(9), 1174–1233. https://doi.org/10.21273/hortsci.57.9.1174
- Long, S., Zhao, X., Shangguan, W.-B., & Zhu, W. (2020). Modeling and validation of dynamic performances of timing belt driving systems. *Mechanical Systems and Signal Processing*, 144, 106910. https://doi.org/10.1016/j.ymssp.2020.106910
- Meng, Q., Manghwar, H., & Hu, W. (2022). Study on Supergenus Rubus L.: Edible, Medicinal, and Phylogenetic Characterization. *Plants*, 11(9), Article 9. https://doi.org/10.3390/plants11091211
- Monteiro, N. O., Casanova, M. R., Fangueiro, J. F., Reis, R. L., & Neves, N. M. (2023). The biomimetic surface topography of *Rubus fruticosus* leaves stimulate the induction of osteogenic differentiation of rBMSCs. *Biomedical Materials*, 18(3), 035008. https://doi.org/10.1088/1748-605X/acc55f
- Monteiro, N. O., Fangueiro, J. F., & Neves, N. M. (2021). Fabrication of biomimetic patterned PCL membranes mimicking the complexity of *Rubus fruticosus* leaves surface. *Colloids and Surfaces B: Biointerfaces*, 206, 111910. https://doi.org/10.1016/j.colsurfb.2021.111910
- Okpala, I. F., Onyenanu, I. U., Ezechukwu, V. C., & Ilochonwu, C. E. (2025). Performance Optimization of a Locally Developed Charcoal Briquette Machine Using Response Surface Methodology. *Scientific Journal of Engineering, and Technology*, *2*(1), 55–66. https://doi.org/10.69739/sjet.v2i1.486

Validation for Rubus Fruticosus Processing. International Journal of Science and Engineering and

Technology (IJSE), 1(1) 144-164.

- Olisah, C. C., Trewhella, B., Li, B., Smith, M. L., Winstone, B., Whitfield, E. C., Fernández, F. F., & Duncalfe, H. (2024). Convolutional neural network ensemble learning for hyperspectral imaging-based blackberry fruit ripeness detection in uncontrolled farm environment. *Engineering Applications of Artificial Intelligence*, 132, 107945. https://doi.org/10.1016/j.engappai.2024.107945
- Onyenanu, I., Okeke, O., Nwobu, C., Akubuenyi, J., Mgbemeje, A., & Okeke, I. (2023). Development of an Enhanced Biomass Gasifier Charcoal Stove. *International Journal of Innovative Science and Research Technology*, 8, 686–694. https://doi.org/10.5281/zenodo.10043296
- Onyenanu, I. U., & Erhimona, O. G. (2023). (PDF) Design and Fabrication of a Palm Fruit Digester. ResearchGate. https://doi.org/10.17577/IJERTV12IS060172
- Sik, B., Ajtony, Z., Lakatos, E., & Székelyhidi, R. (2024). Wild Blackberry Fruit (*Rubus fruticosus* L.) as Potential Functional Ingredient in Food: Ultrasound-Assisted Extraction Optimization, Ripening Period Evaluation, Application in Muffin, and Consumer Acceptance. *Foods*, 13(5), Article 5. https://doi.org/10.3390/foods13050666
- Thanina, A. C., Mourad, B., & Karim, A. (2015). Antibacterial activity of two extracts from *Rubus fruticosus* L. against resistant pathogens and their antioxidant potential. *African Journal of Microbiology Research*, 9(18), 1255–1262. https://doi.org/10.5897/AJMR2015.7437
- Tu, M. (2024). Community Scientists Survey and Assess Invasive Rubus Spp. In Portland Natural Areas: Management Strategies Against Rubus armeniacus Should Not be Altered Due to the Presence of the Congener Rubus praecox. https://bioone.org/journals/natural-areas-journal/volume-44/issue-1/2162-4399-44.1.27/Community-Scientists-Survey-and-Assess-Invasive-Rubus-Spp-in-Portland/10.3375/2162-4399-44.1.27.full
- Ukwu, N. O., Onyenanu, I. U., & Owuama, K. C. (2024). Development of a Low-Cost Banana Fiber Extractor. *International Journal of Innovative Science and Research Technology* (*IJISRT*), 1672–1681., 1672–1681. https://doi.org/10.38124/ijisrt/ijisrt/24apr2282
- Wairegi, L. (2024). *Rubus fruticosus* (blackberry). *CABI Compendium*, *CABI Compendium*, 47995. https://doi.org/10.1079/cabicompendium.47995
- Yan, C., Zhang, Y., Du, K., Guo, J., He, J., Li, J., & Chang, Y. (2021). A ball mill-assisted vortex-enhanced matrix solid-phase dispersion method for the extraction and determination of five phenolic compounds from *Rubi Fructus* by high-performance liquid chromatography. *SEPARATION SCIENCE PLUS*, 4(5), 211–221. https://doi.org/10.1002/sscp.202000110

Technology (IJSE), 1(1) 144-164.